JOURNAL OF APPLIED ELECTROCHEMISTRY **28** (1998) 1157–1166

A model for Kolbe electrolysis in a parallel plate reactor

M. T. HICKS,[1] P. S. FEDKIW*

Department of Chemical Engineering, North Carolina State University Raleigh, NC 27695-7905, USA

Received 17 August 1997; accepted in revised form 27 January 1998

A parallel-plate reactor model is developed for the Kolbe electrolysis of acetate to ethane and carbon dioxide with hydrogen evolution as the counterelectrode reaction. The parallel-plate reactor is considered to consist of three zones: a turbulent bulk region in which streamwise convection is the dominant mass-transport mechanism (plug-flow model) and a thin diffusion layer at each electrode where diffusion and migration mass transport are dominant (Nernst diffusion-layer model). The acetic acid solution is supported with sodium hydroxide, and the reactor is under steady cell-potential control. Gaseous products are tracked by a hypothetical gas layer which increases in thickness in the streamwise direction. The gas phase is assumed to be an ideal, three-component mixture of hydrogen, carbon dioxide and ethane; the liquid phase consists of acetate, proton, acetic acid, and sodium and hydroxyl ions. The model predicts streamwise profiles of concentration, current density, gas-void fraction, and gas and liquid velocities in addition to reactant conversion, and cell-polarization characteristics. The average current density exhibits a maximum at a base-to-acid ratio of 0.96 due to the weak-acid/strong-base chemistry and a broad maximum at an interelectrode spacing of 0.37 cm resulting from minimized ohmic losses.

Keywords: *Kolbe electrolysis*, *parallel plate reactor*, *model*

List of symbols

A_i	constants used in Equation (C.1)
b_a	anodic Tafel constant for acetate Kolbe reaction (V)
b_c	cathodic Tafel constant for hydrogen evolution (V)
c_A	stoichiometric concentration of acetic acid (mol cm^{-3})
c_B	stoichiometric concentration of sodium hydroxide (mol cm^{-3})
C_i	concentration of species i (mol cm^{-3})
$C_{1,ref}$	reference proton concentration (mol cm^{-3})
$C_{2,ref}$	reference acetate concentration (mol cm^{-3})
$D_{app,a}$	apparent diffusivity in anode diffusion-layer (cm^2 s^{-1})
$D_{app,c}$	apparent diffusivity in cathode diffusion-layer (cm^2 s^{-1})
D_i	diffusivity of species i (cm^2 s^{-1})
E_{dec}	decomposition potential (V)
$E_{eq,a}$	equilibrium potential for acetate Kolbe reaction (V)
$E^\circ_{eq,a}$	standard open-circuit potential for acetate Kolbe reaction (V)
$E_{eq,c}$	equilibrium potential for hydrogen evolution (V)
$E^\circ_{eq,c}$	standard open-circuit potential for hydrogen evolution (V)
f	gas–void fraction, δ_G/δ
f_{avg}	average gas–void fraction in reactor
F	Faraday constant (96 487 C mol^{-1})
H	electrode height (cm)
i	current density (A cm^{-2})
$i(0)$	inlet current density (A cm^{-2})
i^*	$i/i(0)$
i_{avg}	average current density in reactor (A cm^{-2})
$i_{o,a,ref}$	exchange current density of acetate Kolbe reaction at reference concentration (A cm^{-2})
$i_{o,c,ref}$	exchange current density of hydrogen evolution at reference proton concentration (A cm^{-2})
IR	ohmic-voltage loss (V)
k	mass-transfer coefficient (cm s^{-1})
K_a	acetic acide dissociation equilibrium constant (mol cm^{-3})
K_w	water ionization equilibrium constant (mol^2 cm^{-6})
N_i	flux of species i (mol cm^2 s^{-1})
P	pressure (atm)
R	gas constant (82.05 atm cm^3 mol^{-1} K^{-1})
R_{ij}	molar volumetric production rate of species i in reaction j (mol cm^{-3} s^{-1})
Re	Reynolds number $= 2v_L\delta/\nu$
q_a	reaction order of acetate in acetate Kolbe reaction
q_c	reaction order of proton in hydrogen evolution
Sc	Schmidt number $= \nu/D_{app}$
Sh	Sherwood number $= 2k\delta/D_{app}$
T	temperature (K)

[1]Present address: 3M Chemicals, St Paul MN, 551440-1000.

*Author to whom correspondence should be addressed.

0021-891X

v_o inlet solution velocity (cm s^{-1})
v_G gas velocity (cm s^{-1})
v_G^* v_G/v_o
v_L liquid velocity (cm s^{-1})
v_L^* v_L/v_o
V_a anode potential (V)
V_c cathode potential (V)
V_T applied cell potential (V)
x streamwise coordinate (cm)
y direction normal to electrode surface (cm)
z_i charge number of species i

Greek symbols
α gas–liquid slip ratio $= v_G/v_L$
δ interelectrode spacing (cm)
δ_a anode diffusion-layer thickness (cm)
δ_c cathode diffusion layer thickness (cm)
δ_G equivalent gas-layer thickness (cm)
κ solution conductivity (S cm^{-1})
η_a anode overpotential (V)
η_{δ_a} anode diffusion overpotential (V)
η_c cathode overpotential (V)
η_{δ_c} cathode diffusion overpotential (V)
ϕ_j solution potential at y coordinate j (V)
ρ solution resistivity (Ω cm)
ρ_o solution bubble-free resistivity (Ω cm)
ν solution kinematic viscosity (cm^2 s^{-1})

Subscripts
1 proton
2 acetate
3 acetic acid
4 hydroxyl
5 sodium ion
b bulk conditions
ref reference conditions
s surface conditions

Superscripts
° stoichiometric concentration

1. Introduction

The Kolbe reaction, that is, the anodic oxidation of the carboxylate moiety in an organic acid with subsequent decarboxylation and coupling to yield a dimer, is an under utilized electrochemical technology. Presently, the Kolbe reaction in a parallel-plate reactor is an important step in the production of sebacic acid from monomethyl adipate [1, 2]. As a means to promote the use and development of the Kolbe reaction, we developed and present below a mathematical model of Kolbe electrolysis in a parallel-plate electrochemical reactor under the condition of turbulent flow. The model incorporates mass-transfer resistance, electrode kinetics, variations in the ionic conductivity due to concentration and bubble effects [3], and homogeneous chemical equilibrium. As a vehicle for illustrative purposes, the model was applied to the Kolbe reaction of acetate

$$2\ CH_3COO^- \rightarrow CH_3CH_3 + 2\ CO_2 + 2\ e^- \qquad (1)$$

in an acetic acid/sodium hydroxide solution at a fixed cell potential, with proton reduction to hydrogen gas

$$2\ H^+ + 2\ e^- \rightarrow H_2 \qquad (2)$$

as the counterelectrode reaction. To our knowledge, there is only one parallel-plate reactor model of Kolbe electrolysis [4]. However, this model assumes a constant bubble-free resistivity and neglects mass-transfer resistance; limitations which are not present in our work.

The present model is used to determine the effects of operating parameters (e.g., cell potential, inlet solution velocity and composition, and interelectrode spacing) on cell performance, and provides a framework to model the Kolbe reaction of other chemicals. Optimization studies are not reported because: (i) acetate oxidation was chosen for illustrative purposes only (i.e., ethane production via acetate oxidation is not envisioned to be an economical viable process), and (ii) optimal operating conditions are reactant dependent (e.g., the optimal conditions for the Kolbe reaction of monomethyl adipate will be different than that for oxidation of acetate).

2. Model development

The electrochemical cell under consideration (Fig. 1(a)) is a vertical parallel-plate reactor of height H and interelectrode spacing δ operating under turbulent-flow conditions. The feed solution enters at velocity v_o and is an aqueous mixture of acetic acid and sodium hydroxide of stoichiometric concentration c_A and c_B, respectively. In the development presented below, five species are numerically indexed for notational convenience: (1) proton (H^+); (2) acetate (CH_3COO^-); (3) acetic acid (CH_3COOH); (4) hydroxyl (OH^-); and (5) sodium (Na^+). The model assumes steady-state and isothermal operation, and dilute-solution theory and electroneutrality apply (i.e., double-layer effects are insignificant), in addition to the following considerations:

(a) The evolved gaseous products are assumed to be ideal and are tracked by a hypothetical gas layer of thickness δ_G which increases in the streamwise direction (Fig. 1(b)); simultaneously, the liquid flows in a hypothetical liquid layer $\delta - \delta_G$ which decreases in thickness. This hypothetical gas layer does not block ionic flow, but rather defines an equivalent gas layer thickness as if all bubbles coalesced at any streamwise position. The gas layer increases the local ionic resistance which is accounted for via the Bruggeman equation [3]

$$\rho = \rho_o(1 - f)^{-1.5} \qquad (3)$$

where ρ, ρ_o and f are explained at the outset. Our approach is similar to that used by Funk

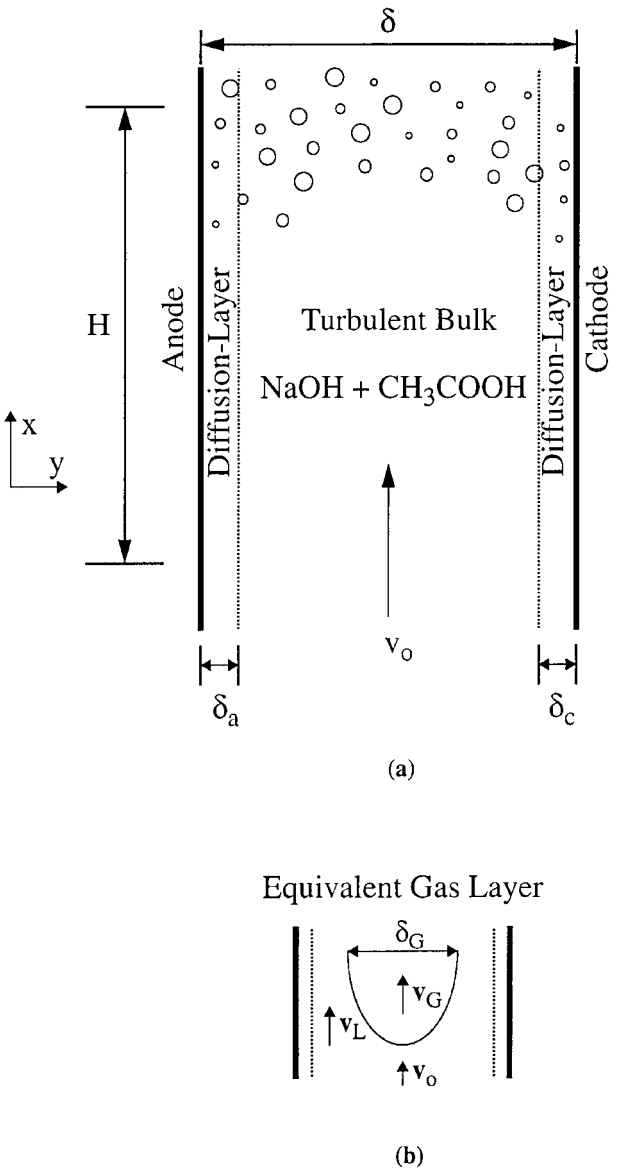

Fig. 1. (a) Schematic of parallel-plate reactor with electrodes oriented vertically; (b) Equivalent gas-layer used in the parallel-plate reactor model.

and Thorpe [5] who modelled a parallel-plate water electrolyser.

(b) The reactor consists of three zones: a turbulent bulk region in which mass transport is by convection only (plug-flow model), and a thin diffusion-layer at each electrode where mass transport is by diffusion and migration (Nernst diffusion-layer model). The thickness of the anode and cathode diffusion layers is δ_a and δ_c, respectively, and is calculated at each streamwise position from a mass-transfer coefficient correlation [6], as described in Appendix A.

(c) The current density is unidirectional and normal to the streamwise flow; consequently, the current density is constant at a given streamwise position.

(d) A single electrochemical reaction occurs at each electrode: Kolbe electrolysis of acetate at the anode and hydrogen evolution at the cathode.

(e) Tafel-like kinetics of the form

$$i_j = i_{o,j,ref}\left[\frac{C_{i,s}}{C_{i,ref}}\right]^{q_j}\exp\left(\frac{\eta_j}{b_j}\right) \tag{4}$$

govern the kinetics of both reactions. The symbols are as listed at the outset. q is the reaction order, and subscripts j, ref and s indicate anode or cathode and reference or surface conditions, respectively.

(f) The cell voltage (V_T) is constant along the cell and is the sum of the thermodynamic decomposition potential (E_{dec}), anode overpotential (η_a), anode diffusion potential (η_{δ_a}), ohmic voltage drop (IR), cathode diffusion potential ($-\eta_{\delta_c}$), and cathode overpotential ($-\eta_c$); that is

$$\begin{aligned} V_T &= E_{dec} + \eta_a + \eta_{\delta_a} + IR - \eta_{\delta_c} - \eta_c \\ V_T &= (E_{eq,a} - E_{eq,c}) + (V_a - E_{eq,a}) \\ &\quad + (\phi_a - \phi_{\delta_a}) + (\phi_{\delta_a} - \phi_{\delta-\delta_c}) \\ &\quad - (\phi_c - \phi_{\delta-\delta_c}) - (V_c - E_{eq,c}) \end{aligned} \tag{5}$$

where $E_{eq,a}$ and $E_{eq,c}$ are the equilibrium potentials for the anode and cathode reactions, respectively, calculated from the Nernst equation, $V_a - E_{eq,a}$ and $V_c - E_{eq,c}$ are the anode and cathode overpotentials, respectively, and ϕ_j is the solution potential at y coordinate j; for example ϕ_a is the solution potential at the anode surface.

(g) The two homogeneous chemical reactions, acetic acid dissociation

$$CH_3COOH \rightleftharpoons H^+ + CH_3COO^- \tag{6}$$

and water ionization

$$H_2O \rightleftharpoons H^+ + OH^- \tag{7}$$

are assumed to be at equilibrium throughout the cell with concentrations related by the acetic acid dissociation constant K_a

$$K_a = C_1C_2/C_3 \tag{8}$$

and the water ionization constant K_w

$$K_w = C_1C_4 \tag{9}$$

The governing differential and algebraic equations are summarized in Appendix B. The governing equations for the bulk solution and diffusion layers are provided in greater detail in [4] and [7], respectively. Note: unlike reference [4], the bubble-free solution resistivity is not constant; instead, experimental data [8] relating the solution conductivity to the sodium hydroxide and acetic acid concentration were empirically correlated (Appendix C). The details of the method of solution are provided in Appendix D.

3. Results and discussion

The parameters used in the calculations are listed in Table 1, unless otherwise noted. The thermodynamic and kinetic constants were obtained from the literature. The gas–liquid slip ratio α was set equal to unity based on Funk and Thorpe's [5] work with hydrogen

Table 1. Parameter values for simulations

$D_1 = 9.312 \times 10^{-5}$ cm^2 s^{-1} [18]
$D_2 = 1.089 \times 10^{-5}$ cm^2 s^{-1} [18]
$D_3 = 0.97 \times 10^{-5}$ cm^2 s^{-1} [9]
$D_4 = 5.260 \times 10^{-5}$ cm^2 s^{-1} [18]
$K_a = 1.8 \times 10^{-8}$ mol cm^{-3}
$K_w = 1.0 \times 10^{-20}$ mol^2 cm^{-6}
$[CH_3COOH]^\circ = 1 \times 10^{-3}$ mol cm^{-3}
$[NaOH]^\circ = 0.65 \times 10^{-3}$ mol cm^{-3}
$\delta = 1$ cm
$H = 100$ cm
$V_T = 6$ V
$P = 1$ atm
$T = 348$ K
$v_o = 20$ cm s^{-1}
$v = 3.88 \times 10^{-3}$ cm^2 s^{-1}(water)
$\alpha = 1$
$C_{1,ref} = 1 \times 10^{-3}$ mol cm^{-3} [19]
$C_{2,ref} = 1 \times 10^{-3}$ mol cm^{-3} [20]
$E^\circ_{eq,a} = 0.396$ V [20]
$E^\circ_{eq,c} = 0.0$ V [19]
$b_a = 0.072$ V [20]
$b_c = 0.013$ V [19]
$q_a = 0.6$ [21]
$q_c = 0.5$ for pH $\leq 4, 0.0$ for pH > 4 [22]
$i_{o,a,ref} = 1.9 \times 10^{-18}$ A cm^{-2} (calculate from Fig. 1 in [20])
$i_{o,c,ref} = 1.0 \times 10^{-3}$ A cm^{-2} [19]

and oxygen mixtures in water. The reactor geometrical parameters were set to realistic values.

3.1. *Equilibrium concentrations and current density at reactor inlet*

Figure 2 shows the equilibrium concentration of proton, acetate, acetic acid, and hydroxyl at the reactor inlet as a function of the base-to-acid ratio for a stoichiometric acetic acid concentration of 10^{-3} mol cm^{-3}. Adding sodium hydroxide increases the degree of acetic acid dissociation and, hence, acetate concentration. Clearly, the sodium hydroxide concentration is critical in setting concentrations in the liquid phase, especially as the base-to-acid ratio approaches unity due to the large change in solution pH.

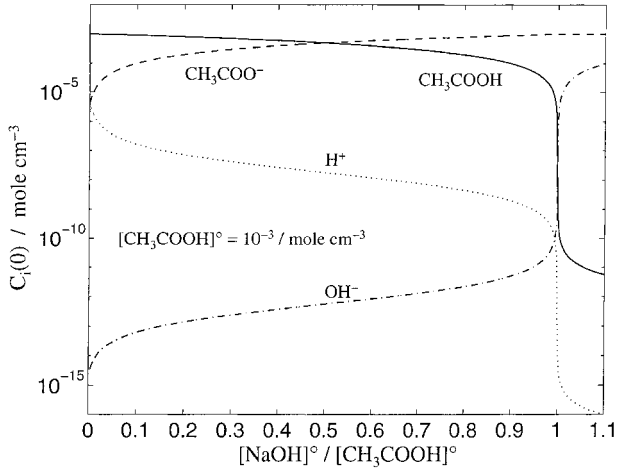

Fig. 2. Equilibrium concentrations as a function of the base-to acid ratio.

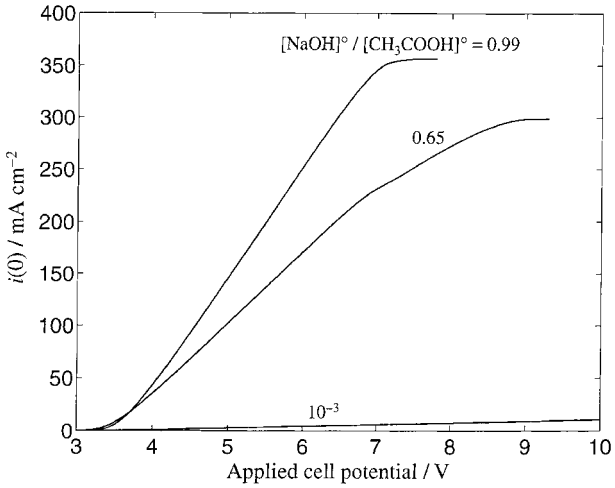

Fig. 3. Inlet current density $i(0)$ as a function of applied cell potential for three feed base-to-acid ratios.

Figure 3 shows the current density $i(0)$ at reactor inlet as a function of the applied cell potential for three different base-to-acid ratios. As the cell potential is increased, the current density increases to its mass-transport limited value which is dependent on the sodium hydroxide concentration due to migration effects [7]. For all base-to-acid ratios, the current is limited by mass transport in the anode diffusion layer. The cathode reaction (hydrogen evolution) is not mass-transport limited because reduction of water effectively occurs as a result of incorporating water dissociation into the model. When there is little sodium hydroxide present, ohmic losses dominate due to the low conductivity of the solution and the current at 6 V, for example, is only a small fraction (2%) of the mass-transport limited current. As the base-to-acid ratio is increased above the lowest value shown (10^{-3}), the solution conductivity increases and likewise the current. The inflection at 7 V for the base-to-acid ratio of 0.65 originates from changes in the concentration profiles within the anode diffusion-layer. At a potential less than 7 V essentially only acetate is depleted throughout the anode diffusion-layer, while at a potential greater than 7 V, both acetate and acetic acid are depleted. The inflection does not occur for the base-to-acid ratio of 0.99 because acetic acid is essentially completely dissociated, and it is not observed for the base-to-acid ratio of 10^{-3} because of ohmic distortion (i.e., the current is too low to observe the effect).

3.2. *Concentration, gas–void fraction, current density, and velocity profiles*

Bulk concentration profiles in the streamwise direction for a cell potential of 6 V and a feed base-to-acid ratio of 0.65 are shown in Fig. 4. Although acetate is consumed at the anode, its concentration remains essentially constant due to the buffering effect of the undissociated acetic acid which does, however, decrease in concentration. Figure 4 also indicates that the solution pH increases in the streamwise direction,

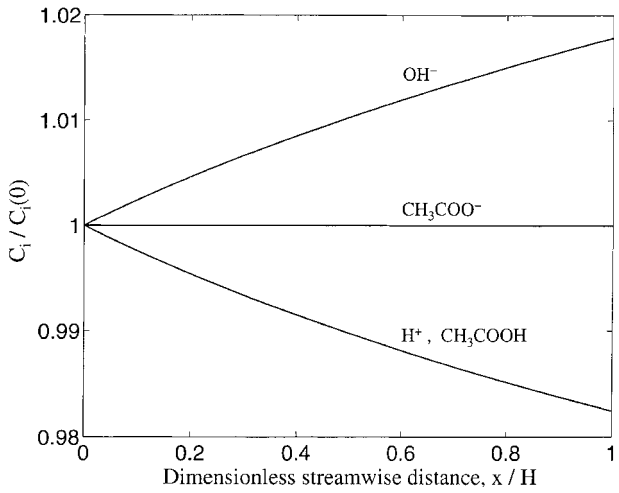

Fig. 4. Streamwise variation of the liquid phase concentrations.

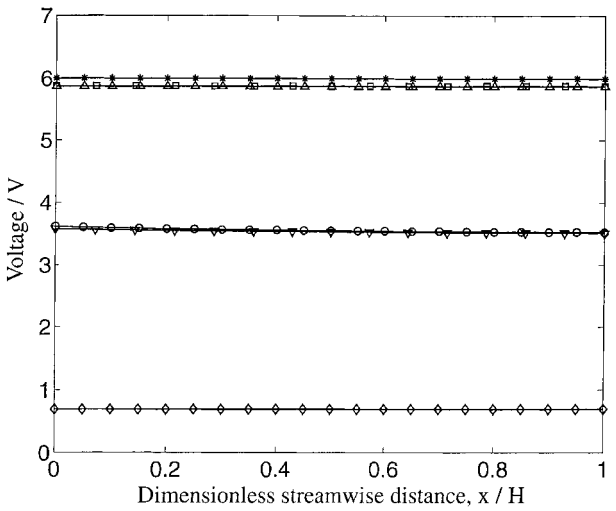

Fig. 6. Streamwise variation of potential distribution for a 6 V cell potential. Key: (◇) E_{dec}; (▽) $\eta_a + E_{dec}$; (□) $\eta_{\delta_a} + \eta_a + E_{dec}$; (△) $IR + \eta_{\delta_a} + \eta_a + E_{dec}$; (□) $= -\eta_{\delta_a} + IR + \eta_{\delta_a} + \eta_a + E_{dec}$; (∗) $-\eta_c - \eta_{\delta_c} + IR + \eta_{\delta_a} + \eta_a + E_{dec}$.

which results from two effects: (i) proton consumption at the cathode, and (ii) the decrease in proton concentration in equilibrium with the decreased acetic acid content. None of the species' concentration change significantly which indicates that the reactor is operating in differential mode at the chosen conditions, that is, low conversion per pass. Figure 5 shows the corresponding variations in current density, gas–void fraction, and gas and liquid velocity. The gas–void fraction increases from 0 to 0.26 due to combined gas evolution from the anode and cathode. The increased gas–void fraction increases: (i) the solution resistance, thus lowering the local current density, and (ii) the liquid velocity because of the reduced cross-sectional area for flow. The gas velocity increases because of the increased gas volumetric flow rate. As a consequence of setting the slip ratio to unity, the liquid and gas velocity are equal.

3.3. *Cell potential balance*

The cell potential distribution in the streamwise direction is shown in Fig. 6 for the set of conditions used to construct Figs 4 and 5. At any streamwise position, the sum of the decomposition potential E_{dec}, the anode overpotential η_a, the anode diffusion potential η_{δ_a}, the ohmic-voltage drop IR, the cathode diffusion potential $-\eta_{\delta_c}$, and the cathode overpotential $-\eta_c$ is 6 V. The decomposition potential is essentially constant because of the small changes in the bulk concentrations. Because of the low exchange current density for the acetate Kolbe reaction, the anode overpotential consumes most of the applied potential, although the ohmic-voltage loss is also substantial. For example, at the reactor inlet, the anode overpotential is about 2.9 V and the ohmic-voltage loss is about 2.2 V. The anode overpotential decreases in the streamwise direction while the ohmic-voltage loss increases due to the increased solution resistance. The anode and cathode diffusion overpotentials, and cathode overpotential are minor contributors to the 6 V cell potential.

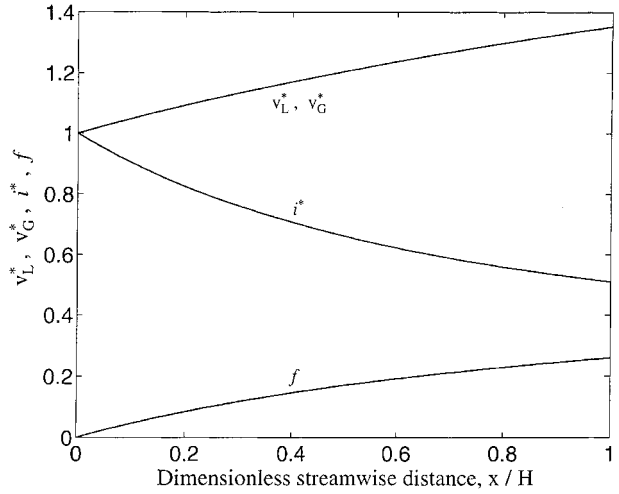

Fig. 5. Streamwise variation of gas velocity v_G^*, liquid velocity v_L^*, current density i^* and gas–void fraction f.

3.4. *Parametric studies*

We have used the model to investigate the effects on the average current density of varying the inlet solution velocity, interelectrode spacing, and feed base-to-acid ratio. The results are shown in Figs 7 to 10. The parameters used in these simulations are the same as those listed in Table 1, unless otherwise noted.

The average current density increases with inlet solution velocity and asymptotically approaches the inlet current density (Fig. 7). The average current density increases because the gas removal rate increases with inlet solution velocity, thus lowering the gas–void fraction and the solution resistivity. The change in the average current density is most rapid when the inlet solution velocity is low ($v_o <$ 20 cm s^{-1}), because the total acetate conversion is at its highest value. The infection at 155 cm s^{-1} in all three calculated quantities is unexpected but can be explained. The average current density, and hence the volumetric production rate of gas, is nearly constant

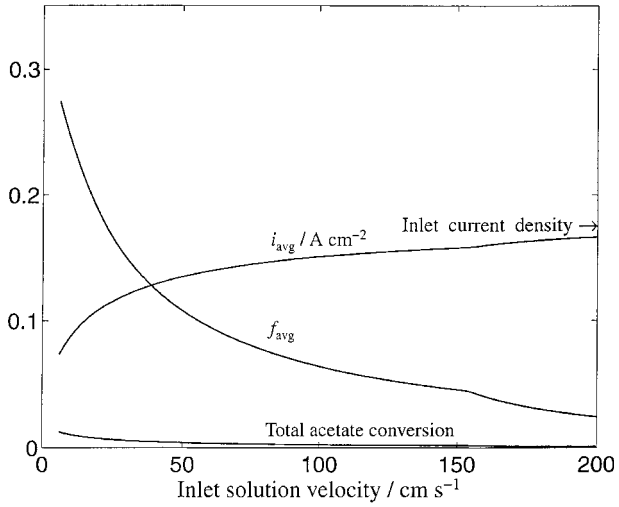

Fig. 7. Effect of varying the inlet solution velocity on i_{avg}, f_{avg}, and total acetate conversion.

for an inlet solution velocity between 100 to 150 cm s^{-1}. Simultaneously, the volumetric removal rate of gas increases with solution velocity. The inflection at 155 cm s^{-1} results from the volumetric gas removal rate being greater than the production rate which decreases the average gas–void fraction and, hence, solution resistance, thus increasing the average current density. For the specified geometric cell parameters, the inlet solution velocity must be greater than 5.8 cm s^{-1} to use the mass-transfer coefficient correlation (i.e., $Re > 2100$ for turbulent-flow) [6], which defines the lower limit used in these calculations.

The effect of interelectrode spacing δ on the average current density, average gas–void fraction, and total acetate conversion is shown in Fig. 8. The average current density has a broad maximum at an interelectrode spacing of 0.37 cm. If the interelectrode spacing is less than 0.37 cm, the current density decreases because of the increasing gas–void fraction which lowers solution conductivity. But if the interelectrode spacing in greater than 0.37 cm, the current density decreases because of the ohmic loss associated with the longer ionic pathway. Both the average gas–void fraction and total acetate conversion decrease monotonically with interelectrode spacing, since the ratio of electrode area to volumetric flow rate decreases. To use the mass-transfer coefficient correlation for the given geometric cell parameters, δ must be greater than 0.29 cm [6].

The effect of the feed base-to-acid ratio on the average current density is shown in Fig. 9. As the ratio increases from zero, the bubble-free solution resistivity decreases and the average current density increases. However, as the base-to-acid ratio approaches unity, the average current density rapidly decreases because the acid is becoming more neutralized and the greater ionic content lowers the migration flux within the diffusion-layers [7].

Figure 10 illustrates the effect of applied cell potential on the average current density at three feed base-to-acid ratios. The average current density increases with cell potential. For any given potential, the average current density at a base-to-acid ratio of 10^{-3} is the lowest of the three due to the low conductivity of the solution. For potentials greater than 3.7 V, the average current density for a base-to-acid ratio of 0.99 is greater than the average current density for a base-to-acid ratio of 0.65 due to the higher inlet current density (Fig. 3). However, at potentials greater than 6 V the difference between the two currents decreases because of the higher average gas–void fraction for the base-to-acid ratio of 0.99. The limiting current for each base-to-acid ratio is different because the migration flux within the diffusion layers varies with sodium hydroxide concentration [7].

3.5. *Effect of mass transfer resistance and the concentration dependence of bubble-free resistivity*

Figure 11 compares the inlet current density $i(0)$ as a function of applied cell potential with and without

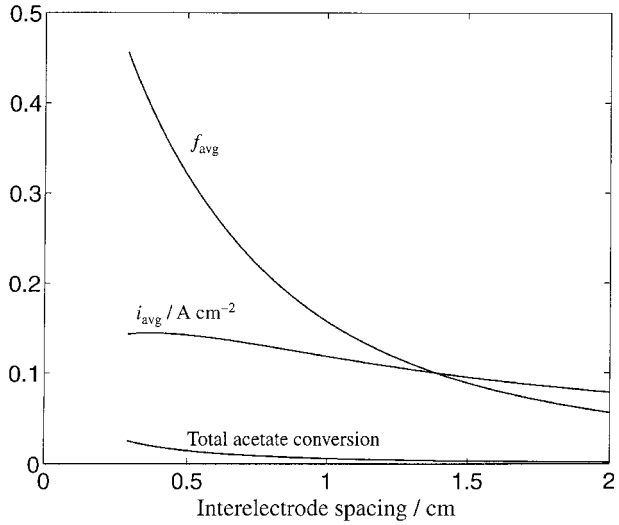

Fig. 8. Effect of varying the interelectrode spacing on i_{avg}, f_{avg}, and total acetate conversion.

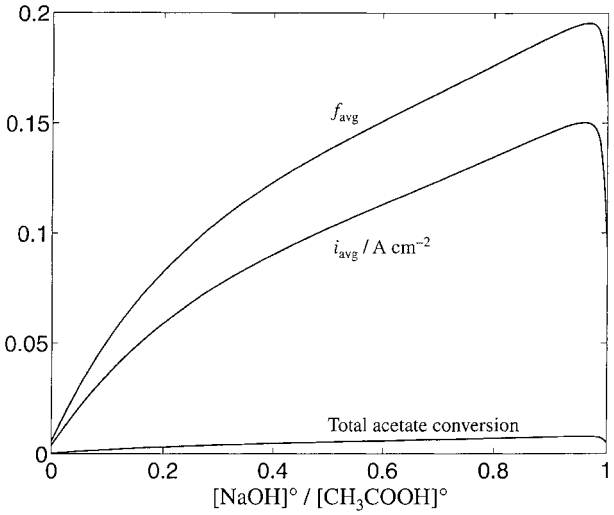

Fig. 9. Effect of varying the feed base-to-acid ratio on i_{avg}, f_{avg}, and total acetate conversion.

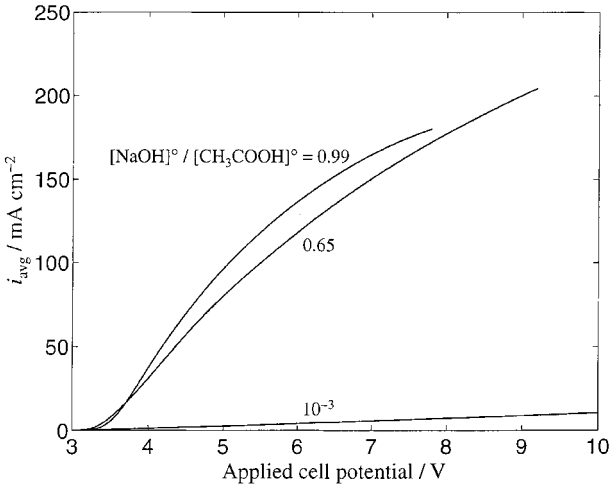

Fig. 10. Average current density i_{avg}, as a function of applied cell potential for three feed base-to-acid ratios.

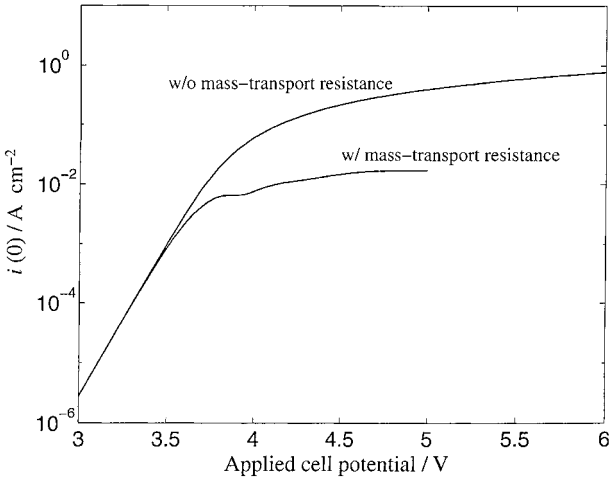

Fig. 11. Effect of mass-transfer resistance on the inlet current density $i(0)$ as a function of applied potential. $[CH_3COOH]^\circ = 1 \times 10^{-4}$ mol cm^{-3}; $[NaOH]^\circ = 5 \times 10^{-5}$ mol cm^{-3}; $T = 298$ K; constant bubble – free resistivity = 2.5 Ω cm.

mass-transport resistance taken into consideration. At low cell voltages, the two models are in agreement. The current calculated from the model without mass-transport resistance [4] is at least an order of magnitude greater than the current calculated from the model with mass-transport resistance for potentials greater than 4 V. This result indicates that the reactor performance (i.e., average current density and total acetate conversion) for the mass-transport resistance model will be less than the calculated in its absence. Previously, we argued that mass-transport resistance should only a concern when the solution velocity is low due to the buffering effect of the undissociated acetic acid [4]. However, as illustrated in Fig. 11, this is not the case at potentials greater than 3.5 V. One must remember that both acetate and undissociated acetic acid are electrochemically active due to the homogeneous chemical equilibrium. As a result, the total acetate content (acetate and undissociated acetic acid) is the reactant for the Kolbe reaction. Although the undissociated acetic acid buffers the acetate concentration, the total acetate concentration is reduced.

In the previous model by Yan *et al.* [4], we assumed a constant bubble-free resistivity of 2.5 Ω cm for the reactor feed at 298 K consisting of 1×10^{-4} mol cm^{-3} acetic acid with 5×10^{-5} mol cm^{-3} sodium hydroxide. Because of the low conversion per pass in the mass-transport resistance model, the assumption of a constant bubble-free resistivity appears realistic. In the model with mass-transport resistance, the bubble-free resistivity only varied at most by 0.02%. A much more important effect was underestimating the bubble-free resistivity. Recent experimental data [8] indicates that the actual bubble-free resistivity is 249 Ω cm. The large bubble-free resistivity lowers the current in comparison to our previous calculations.

4. Summary

A mathematical model has been developed to study Kolbe electrolysis in a parallel-plate reactor operating under turbulent-flow. The model has been applied to Kolbe electrolysis of acetate in an acetic acid/sodium hydroxide solution, but can be used as a basis to study any Kolbe reaction by applying the proper physical and electrochemical constants. The model incorporates electrode kinetics, mass-transfer resistance, homogeneous chemical equilibrium, and variations in ionic conductivity due to concentration and bubble effects. Results indicate that the current density decreases in the streamwise direction due to increased solution resistance resulting from gas evolution. The inlet current density increases with applied cell potential to the mass-transport limited value, which is limited by transport in the anode diffusion layer. At a 20 cm s^{-1} inlet solution velocity the reactor is operating in differential mode (total acetate conversion of 0.6%). Parametric studies indicate that the average current density increases with inlet solution velocity and asymptotically approaches the inlet solution current density. The average current density exhibits a broad maximum at an interelectrode spacing of 0.37 cm. There is also a distinct maximum in the average current density at a base-to-acid ratio of approximately 0.96.

Acknowledgement

This work was sponsored by the DuPont Educational Aid Program. We thank Dr Clarence Law of DuPont for his support and for providing the conductivity data referenced in Appendix C.

Appendix A: Diffusion-layer thickness

The diffusion-layer thickness is calculated from the following mass-transfer coefficient correlation [6]

$$Sh = 0.0153\, Re^{0.88} Sc^{0.32} \qquad (A.1)$$

where Sh, Re and Sc represent the Sherwood, Reynolds and Schmidt numbers, respectively, and are defined as

$$Sh = \frac{2k\delta}{D_{app}}$$
$$Re = \frac{2v_L\delta}{v}$$
$$Sc = \frac{v}{D_{app}} \quad (A.2)$$

where k is the mass-transfer coefficient, D_{app} is the apparent diffusion coefficient [9], v_L is the liquid velocity, and v is the solution kinematic viscosity. At the cathode, the apparent diffusivity $D_{app,c}$ is

$$D_{app,c} = (C_{1,b}D_1 + C_{3,b}D_3)/c_A \quad (A.3)$$

where subscript 'b' indicates bulk conditions; while at the anode, the apparent diffusivity $D_{app,a}$ is

$$D_{app,a} = (C_{2,b}D_2 + C_{3,b}D_3)/c_A \quad (A.4)$$

Recalling that k is equal to $D_{app,i}/\delta_i$ [10]. Equation A.1 is rearranged to yield

$$\delta_i = \frac{2\delta}{0.0153} Re^{-0.88} Sc_i^{-0.32} \quad (A.5)$$

where subscript 'i' indicates anode or cathode.

Appendix B: Governing differential and algebraic equations

B.1. *Diffusion-layer (boundary-value problem)*

The steady-state balances are written for each species as

$$\nabla \cdot \boldsymbol{N}_i = R_{i,j} \quad (B.1)$$

where $R_{i,j}$ is the molar production rate of species i per unit volume from the homogeneous chemical reaction j (Reaction 6 or 7). The flux of each species $\boldsymbol{N}_i$ is given by the Nernst–Planck equation with the Nernst–Einstein equation used to relate ionic mobility to the diffusivity

$$\boldsymbol{N}_i = -D_i\left(\nabla C_i + z_i \frac{FC_i}{RT}\nabla\phi\right) \quad (B.2)$$

where the symbols are as listed at the outset. The steady-state material balances are appropriately summed to eliminate $R_{i,j}$. It is assumed that the homogeneous chemical reactions are at equilibrium, thus Equations 8 and 9 are valid, and that the electrolyte is electrically neutral

$$\sum_{i=1}^{5} z_i C_i = 0 \quad (B.3)$$

For both boundaries, the concentrations are presumed to satisfy electronuetrality and the equilibrium relationships. At the diffusion-layer, bulk conditions apply and the potential is arbitrarily set equal to zero. (Note: the bulk concentrations and potential at the diffusion-layer vary with streamwise position. However, since the method of solution uses potential differences, the value of the potential at the diffusion-layer is inconsequential in this model, and the streamwise bulk concentrations are accounted by the turbulent-bulk model, next Section.) At the electrode surface, the flux of nonelectroactive ions is set equal to zero, and the surface concentration of the electroactive species (proton at the cathode and acetate at the anode) is specified as a small fraction of its bulk value. (The actual value is not important because the method of solution adjusts the surface concentration until the correct value is determined for the given operating conditions, as described in Appendix D.) The current is due to the motion of charged species and is calculated as

$$i = F\sum_{i=1}^{5} z_i \boldsymbol{N}_i \quad (B.4)$$

Additional information on the governing equations and their manipulation to solve the boundary-valued problem can be found in [7].

B.2. *Turbulent bulk (initial-value problem)*

The governing equations for proton, acetate, acetic acid, and hydroxyl are acetic acid equilibrium (Equation 8), water ionization (Equation 9), electroneutrality (Equation B.3), and the steady-state total acetate mole balance

$$\frac{d}{dx}[(\delta - \delta_G)(C_2 + C_3)v_L] = -i/F \quad (B.5)$$

Table 2. Bubble-free resistivity coefficients in Equation C1

Temperature/K	A_1	A_2	A_3	A_4	A_5
298	0.331	17.8	−18.0	12.2	0.786
323	0.294	27.8	−27.9	18.3	0.784
348	0.355	41.7	−40.5	26.1	0.789

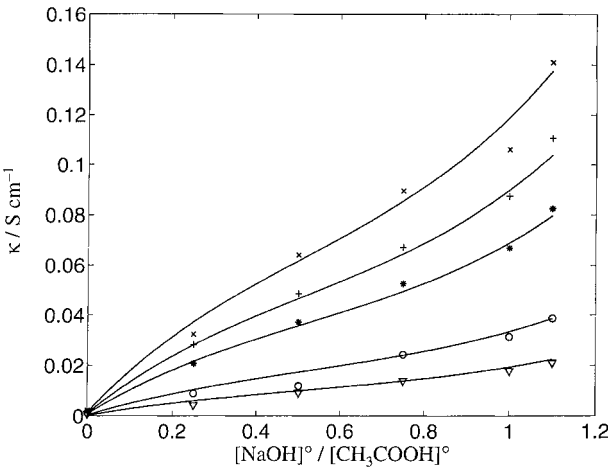

Fig. 12. Acetic acid/sodium hydroxide conductivity as a function of solution composition at 348 K. Symbols: experimental data; lines: calculated using Equation C.1. $[CH_3COOH]^\circ$: (▽) 0.1×10^{-3}, (○) 0.2×10^{-3}, (*) 0.5×10^{-3}, (+) 0.7×10^{-3} and (×) 1.0×10^{-3} mol cm^{-3}.

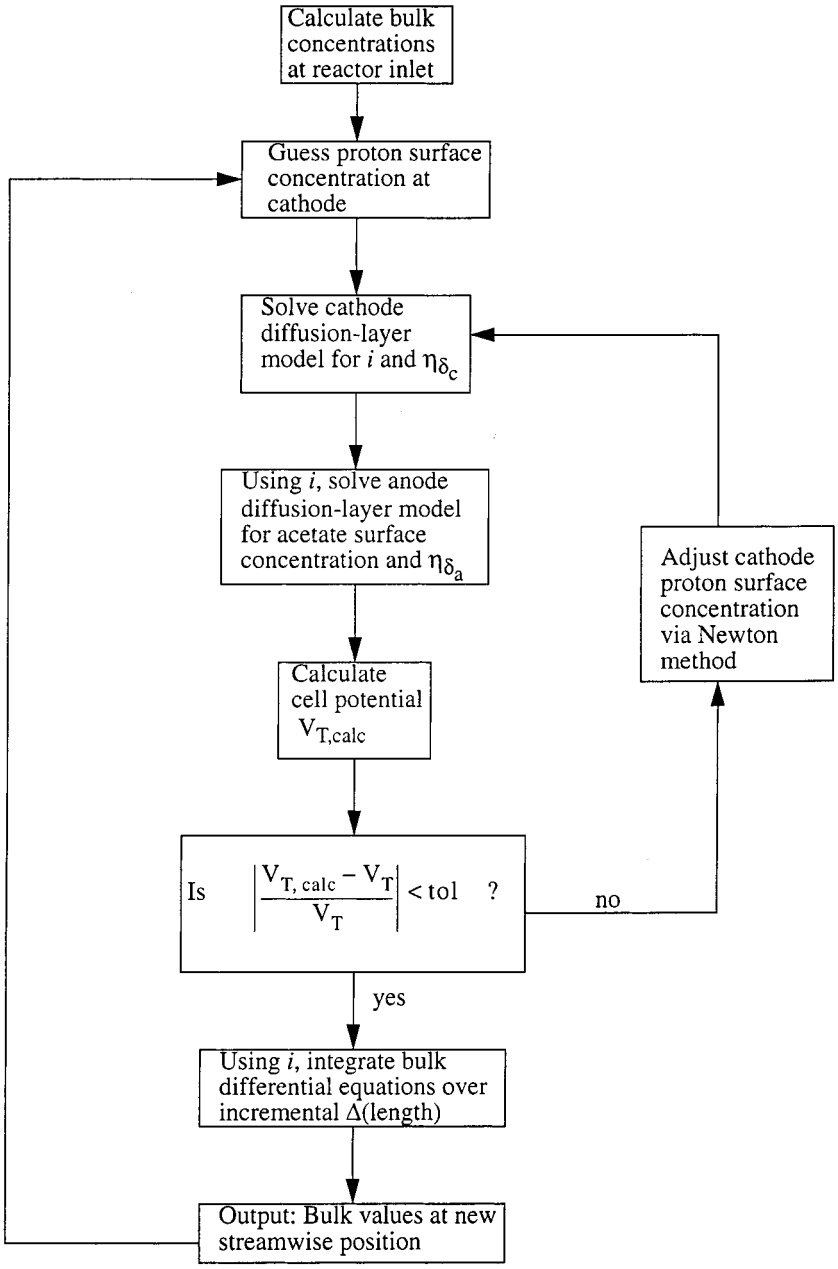

Fig. 13. Algorithm used to solve model equations.

The liquid and gas velocities are obtained by dividing the gas or liquid volumetric flow by the appropriate cross-sectional area. Thus, the gas velocity v_G is

$$\delta_G v_G = 2\frac{RT}{FP}\int_0^x i\,dx \tag{B.6}$$

Assuming constant liquid volumetric flow, the liquid velocity v_L is

$$(\delta - \delta_G)v_L = \delta v_o \tag{B.7}$$

Finally, the slip ratio α is defined as the ratio of the gas to liquid velocity

$$\alpha = \frac{v_G}{v_L} \tag{B.8}$$

The equations are combined to yield three differential equations for proton, acetate, and gas–void fraction [4]. At the reactor inlet, the initial conditions are the bulk proton and acetate concentration, and the gas–void fraction is zero.

Appendix C: Concentration dependence of bubble-free resistivity

Experimental conductivity data were provided by DuPont [8]. The following empirical equation was used to relate the conductivity to the sodium hydroxide and acetic acid composition

$$\kappa = \frac{1}{\rho_o} = \left[A_1 + A_2\left(\frac{c_B}{c_A}\right) + A_3\left(\frac{c_B}{c_A}\right)^2 + A_4\left(\frac{c_B}{c_A}\right)^3\right]c_A^{A_5} \tag{C.1}$$

where κ(S cm^{-1}) is the bubble-free solution conductivity and A_i $i = 1, \ldots, 5$ are constant for a given temperature and are listed in Table 2, although all

results discussed here are at 348 K. At this temperature and for a base-to-acid ratio greater than zero, the maximum absolute percent difference between the calculated and experimental solution conductivity is 45% which occurs at a base-to-acid ratio of 0.5 and an acid concentration of 2×10^{-4} mol cm^{-3}. Figure 12 compares the measured conductivity at 348 K to the correlation.

Appendix D: Method of solution

To solve the two-dimensional system, we have 'divided' the problem into three coupled, one-dimensional problems which represent each region in the reactor: the turbulent core and the two diffusion layers. Essentially, this procedure allows us to solve a boundary-value problem at every streamwise position across each diffusion-layer and an initial-value problem in the turbulent bulk region. The results of each region are coupled by the cell-voltage balance (Equation 5). Our method is similar to that first presented by Alkire and Lisius [11] and later by Lapicque and Stork [12]. Figure 13 illustrates the solution procedure which is described in more detail below.

The inlet bulk concentrations are calculated first and the cathode proton surface concentration at the inlet is guessed. The Q-potential technique [13–17] is used to solve the governing differential and algebraic equations in the cathode diffusion layer with proton concentration as the independent variable. The equations are integrated numerically using *ode*15*s*, a variable step-size integrator in the ODE SUITE of Matlab®, from the bulk proton concentration to the guessed proton surface concentration. The resulting current density and cathode diffusion potential are recorded. Next, using the predicted current density from the cathode diffusion layer, the Q-potential technique is again used to solve the governing differential and algebraic equations in the anode diffusion layer. The equations are integrated numerically using *ode15s* with the Q potential as the independent variable in order to determine the anode acetate surface concentration and the anode diffusion potential. The independent variable in these anode equations is chosen to be the Q potential (different than choice in cathode layer) because the current density is known (as a result of solving the cathode equations for the guessed proton surface concentration) and the Q potential is related to the current density [7]. Next, the cell potential is calculated based on the output from the cathode and anode diffusion-layer models. If the absolute value of the relative percent difference between the calculated and applied cell potential is greater than the specified tolerance (10^{-7}), then the cathode proton surface concentration is adjusted and the procedure repeated until convergence. If the absolute value of the relative percent difference between the calculated and applied cell potential is less than the specified tolerance, the cathode proton surface concentration is recorded and the governing differential equations in the bulk are integrated numerically via the Euler method using the current density from the diffusion-layer model to obtain bulk concentrations and gas–void fraction at a new streamwise position. The previously recorded cathode proton surface concentration is then used as the initial guess at the new streamwise position, and the procedure is repeated for a given streamwise distance.

As a means to test the numerical consistency, the average current density was calculated by three methods: total mole balance on acetate, mole balance on gaseous products and integration of the local current density. The results showed good agreement for the three methods with a maximum deviation of 0.8%.

References

[1] M. Seko, A. Yomiyama and T. Isoya, *Hydrocarbon Processing*, No. 12 (1979) 117.
[2] Y. B. Vassiliev, E. P. Kosvman and G. N. Friedlin, *Electrochim. Acta* **27** (1982) 937.
[3] C. W. Tobias, *J. Electrochem. Soc.* **106** (1959) 833 .
[4] J.-F. Yan, P. S. Fedkiw and C. G. Law, Jr., *J. Appl. Electrochem.* **26** (1996) 175.
[5] J. E. Funk and J. F. Thorpe, *J. Electrochem. Soc.* **116** (1969) 48.
[6] D. A. Dawson and O. Trass, *Int. J. Heat Mass Transfer* **15** (1972) 1317.
[7] M. T. Hicks and P. S. Fedkiw, *J. Electroanal. Chem.* **424** (1997) 75.
[8] C. G. Law, Jr, DuPont Experimental Station, personal communication (1995).
[9] Z. Stojek, M. Ciszkowska, and J. Osteryoung, *Anal. Chem.* **66** (1994) 1507.
[10] D. J. Pickett, 'Electrochemical Reactor Design,' 2nd edn., Elsevier Scientific, New York (1979), p. 64.
[11] R. C. Alkire and J. D. Lisius, *J. Electrochem. Soc.* **132** (1985) 1879.
[12] F. Lapicque and A. Storck, *J. Appl. Electrochem.* **15** (1985) 925.
[13] B. Pillay and J. Newman, *J. Electrochem. Soc.* **140** (1993) 414.
[14] D. R. Baker, M. W. Verbrugge, and J. Newman, *J. Electroanal. Chem.* **314** (1991) 23.
[15] D. R. Baker, M. W. Verbrugge and J. Newman, *J. Electrochem. Soc.* **140** (1993) 2530.
[16] *Idem, Electrochim. Acta* **38** (1993) 1649.
[17] D. R. Baker, *SIAM J. Appl. Math* **53** (1993) 419.
[18] J. Newman, 'Electrochemical Systems,' 2nd edn., Prentice Hall, Englewood Cliffs, NJ (1991), p. 255.
[19] H. H. Uhlig and R. W. Revie, 'Corrosion and Corrosion Control,' 3rd edn., J. Wiley & Sons, New York (1985), p. 44.
[20] A. V. Vijih and B. E. Conway, *Z. Anal Chem.* **224** (1967) 160.
[21] Yu. B. Vassiliev and V. A. Grinberg, *J. Electroanal. Chem.* **336** (1992) 281.
[22] V. S. Bagotzky and N. V. Osetrova, *J. Electroanal. Chem.* **43** (1973) 223.